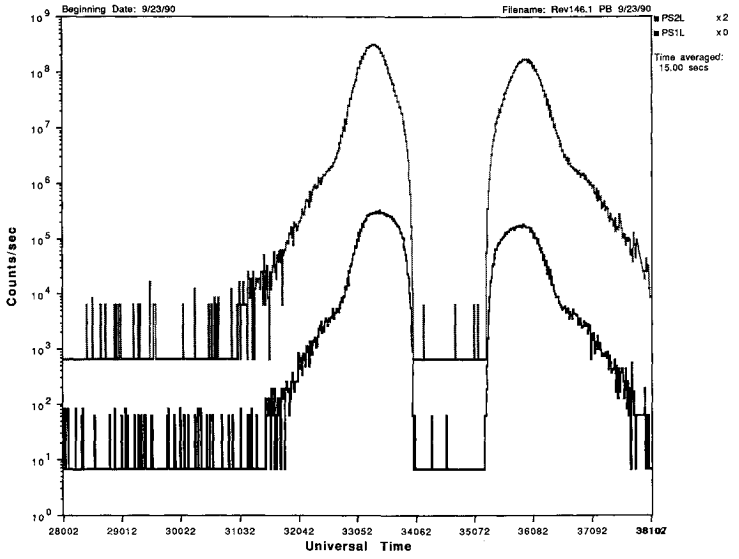

Fig. 2 Data from the low-threshold channels of the two proton switches are shown during the time period around perigee. Note that the top curve is multiplied by 100 in order to separate the two curves. Between ≈ 28,000 and 31,500 s the CRRES spacecraft was above the region containing the energetic protons, and the proton switches were counting cosmic-ray background. The two peaks result from the inbound and outbound legs of the CRESS orbit because the spacecraft goes below the radiation belts before reaching perigee. Note the very low background between the peaks (around perigee) where the geomagnetic field excludes much of the galactic cosmic-ray flux; thus the background count rate is reduced substantially in that region.

Table 1 Calculated approximate geometric factors and energy ranges

Channel identification	Energy range, MeV	Geometric factor, mm^2
PS2L	21-84	3.9
PS2H	23-51	2.6
PS1L	51-107	3.6
PS1H	51-77	2.7

Acknowledgment

This work was supported under Air Force Space Systems Division Contract FO4701-88-0089.

CRRES Low-Energy Magnetospheric Ion Composition Sensor

D. T. Young*
Southwest Research Institute
San Antonio, Texas 78228
and
B. L. Barraclough,† D. J. McComas,†
M. F. Thomsen,† K. McCabe,‡
and R. Vigil‡
Los Alamos National Laboratory
Los Alamos, New Mexico 87545

Introduction

ONE major goal of space plasma physics is understanding the origins, acceleration processes, and transport of mass, momentum, and energy through the Earth's magnetosphere, objectives that are addressed by plasma mass spectrometry. Both the solar wind, consisting predominantly of H^+ and $^4He^{2+}$ ions, and the terrestrial topside ionosphere, which consists primarily of H^+, He^+, O^{2+}, and O^+, contribute to magnetospheric particle populations. Furthermore, many acceleration processes are dependent on the ion mass/charge ratio, as are transport and loss processes.[1,2] The low-energy magnetospheric ion composition spectrometer (LOMICS) instrument described here is designed to distinguish and measure the velocity distributions of all important magnetospheric ion species up to 44 keV per charge.

Instrumental Approach

Most mass spectrometer experiments flown previously on spacecraft have been based on magnetic analysis of ion momentum (see Ref. 3 and references therein). This technique has several practical limitations, most notably an upper limit on ion energy of about 20 keV, as well as limits on time resolution caused by the need to scan the mass spectrum. More recently, time-of-flight (TOF) methods have been used to obtain solar wind, cometary, and magnetospheric composition measurements,[4,5] usually with emphasis at energies above several tens of kilaelectron volts. LOMICS' TOF technique represents an attempt to improve on limitations of both magnetic and earlier TOF devices, and yet still produce a compact instrument capable of high-quality measurements. It is important to keep in mind that the LOMICS design was also constrained by pre-existing restrictions on volume, mass, and power, and by the design of pre-existing high-voltage power supplies.

Instrument Description

Figure 1 is a schematic diagram of the LOMICS sensor. The sensor is mounted, together with the heavy ion telescope (HIT)[6] and their common data processing unit (DPU)[7] and power supplies, in the high-mass sensor-B (HMSB) unit. Microchannel plate (MCP) detectors and other sensitive elements in LOMICS were protected by a hermetically sealed housing and aperture cover. The cover was opened on-orbit four weeks after launch, when spacecraft outgassing was judged to be acceptably low.

LOMICS consists of a conventional 90-deg spherical-section electrostatic analyzer (ESA) followed by a TOF analyzer. The ESA provides ion energy/charge (E/Q) and angular anal-

Received June 21, 1991; revision received Aug. 27, 1991; accepted for publication Sept. 2, 1991.

*Institute Scientist, Department of Space Sciences, Instrumentation and Space Research Division, P.O. Drawer 28510.

†Staff Member, Space Plasma Physics Group, Space Science and Technology Division, Mail Stop D438.

‡Staff Member, Space Instrumentation Group, Space Science and Technology Division, Mail Stop D440.

ysis. The spherical-section ESA field plates are 0.27 cm apart on a mean radius of 5.72 cm with an entrance area of 0.29 cm^2. The TOF analyzer provides a time measurement (between 1 and 103 ns) that is proportional to ion velocity from which ion mass/charge (M/Q) can be determined according to the relationship

$$M/Q = 2[(E/Q + |V_a|) - \Delta E_f](T^2/L^2) \quad (1)$$

where V_a is the TOF acceleration voltage (-10.0 kV), ΔE_f the ion energy per unit charge lost to collisions in the foil, and T the measured flight time over the known length L of the TOF region (2.20 cm). The outer plate is swept over a logarithmic range of positive potential with the inner plate at ground.

Ions enter the ESA through a grounded aperture that collimates the flux to ± 4-deg full width-half maximum (FWHM) in azimuth. Polar angle acceptance is limited to ± 2.5-deg FWHM by the width of the apertures on which the carbon foils are mounted (Fig. 1). The ESA selects ions in the range ~ 20 to 44 keV/e with an energy resolution of 13% FWHM. A single sample requires 0.128 s, and a full logarithmic 32-sample energy sweep is made every 4.096 s. Energy-analyzed ions exiting the ESA are accelerated through a potential of -10.0 kV and then strike one of three carbon foils with a total energy ($E + 10.0Q$) keV. Ions pass through the extremely thin foil (0.5 $\mu g\ cm^{-2}$, about 25 Å thick) and cause one or more secondary electrons to be emitted. The secondaries are accelerated, deflected, and focused by an einzel lens onto a stack of three 25-mm-diam MCPs arranged in a Z-stack configuration. This MCP stack (hereafter referred to as the start-MCP) emits a pulse that starts the TOF timing process. Ions exit the foil with a small energy loss (~ 0.5–1.5 keV depending on incident velocity) and proceed to the corresponding stop-MCP detector that defines one of three polar-angle view directions centered at 0 and ± 30 deg to the satellite spin plane (Fig. 1). The resulting MCP signal stops the TOF measurement, causing the electronics unit to strobe out the time-to-voltage converter and to digitize and process the voltage value (proportional to TOF) as described later. The stop-MCPs are configured in a Z-stack like that of the start-MCP, but with the important difference that the input MCP of each Z-stack is mounted on the TOF housing, which is biased at -10.0 kV, whereas the other two plates in each stack are mounted approximately 1 cm away with their input biased at -1.6 kV relative to ground (Fig. 1). This arrangement decouples the stop-MCP signal from the -10.0 kV of the TOF without the need for bulky high-voltage capacitors. All MCP bias voltages (start and stop) are provided by a single programmable power supply. Individual MCP gain adjustments were made with bias resistors prior to launch.

LOMICS shares the analog-to-digital converter (ADC) that digitizes the TOF voltage for each event, as well as the separate DPU,[7] with the HIT.[6] The LOMICS and HIT alternate every 65.536 s, with LOMICS data read out to telemetry as HIT data is accumulated and vice versa. Thus, although LOMICS operates continuously, the quantity of data returned cycles is between 10 and 100% every 65.536 s. The amplitude of the TOF pulse is digitized with 10-bit resolution in the HMSB electronics unit. Simultaneously with the recognition of a valid TOF event, the ESA plate voltage is sampled and digitized to 5 bits, giving the incident ion energy/charge. In addition, a 2-bit ID code is generated that indicates from which of the three polar directions the incident ion arrived (Fig. 1). The combination of TOF, E/Q, and angle ID constitutes an address code that is sent to the DPU for each event. Because telemetry is not sufficient for handling all data as (TOF, E/Q, ID) addresses, only a fraction (so-called direct events) are returned and then only during a special selectable telemetry mode. In addition to the direct event data, two scalers are incremented for events whose TOF (regardless of E/Q) is between 1 and 22 ns (corresponding roughly to hydrogen) and between 22 and 103 ns (oxygen and heavy ions). Individual MCP count rates from all start and stop detectors are transmitted as singles, i.e., as data that do not require a coincidence. This provides the total event rate used to make dead time corrections to TOF data. A fourth and fifth type of data, the so-called rate scaler and matrix data, are discussed in the following.

The LOMICS TOF and E/Q values are presented to a look-up table that sorts the event into 1 of 32 M/Q bins. The resultant M/Q and polar angle ID values are then used as addresses to increment one of six scaler locations in memory (RAM). The RAM itself can be selectively divided up four different ways (termed pages) to provide either three-dimensional or two-dimensional coverage of predetermined mass and polar angle groups. These scaler data are returned at each of the 32 energy steps taken during a 4.096-s energy sweep, and constitute the main LOMICS data. In addition, all M/Q values are accumulated according to their ID value without regard to E/Q, and stored in another section of RAM for readout every 65.536 s.

LOMICS data handling provides four principal modes of returned data based on four pages of RAM described earlier. It is obvious that with only six rate scalers, the full angle and mass resolution of the instrument cannot be transmitted, viz. 5 M/Q values $\times$ 3 angles requires 15 scalers. The four data modes represent different compromises between angular coverage and species coverage. In the standard mode, mass coverage is emphasized at the expense of angular resolution: counts

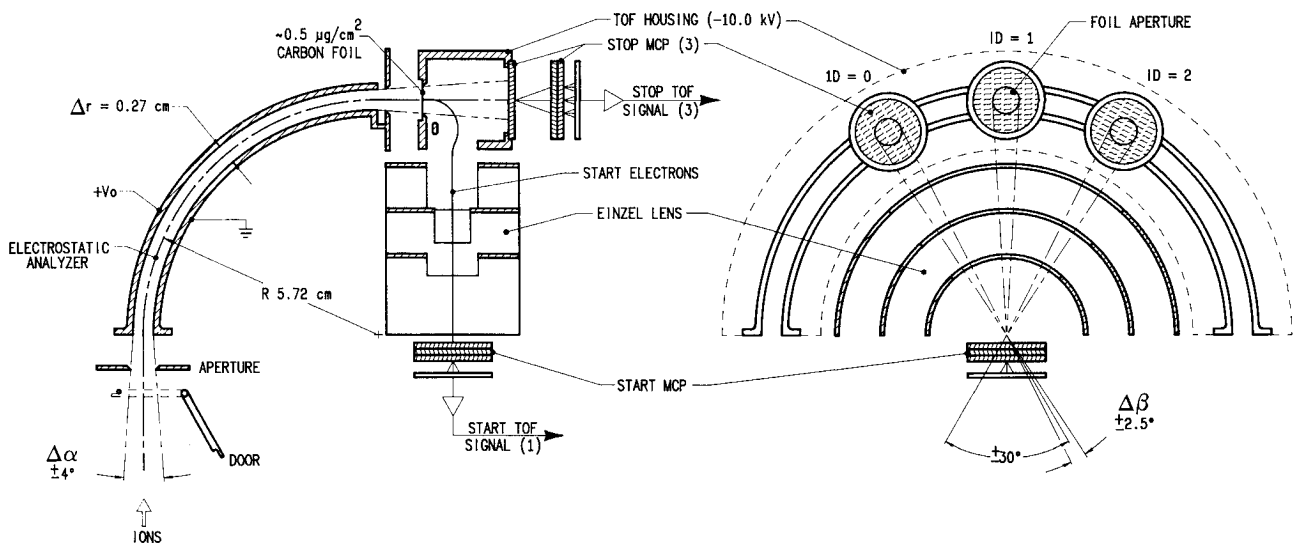

Fig. 1 Schematic diagram of the LOMICS sensor unit.

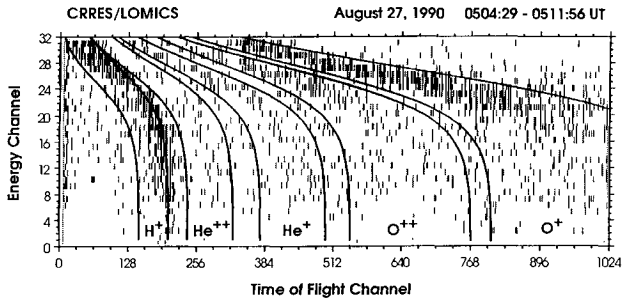

Fig. 2 Flight data from LOMICS with TOF calibration data (curved lines) overlaid on an E/Q vs TOF spectrogram.

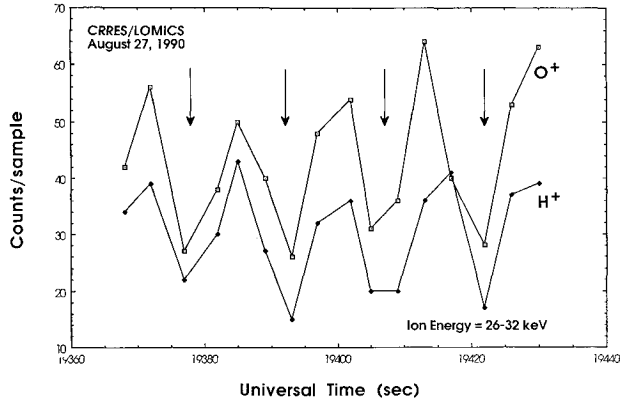

Fig. 3 Spin modulation O^+ and H^+ fluxes in the energy range 26–32 keV.

Table 1 LOMICS calibration summary

Parameter	Detector ID (Fig. 1)	Value	Units
Geometric factor	1	7.0×10^{-5}	cm^2sr eV/eV counts/ion
Geometric factor	0,2	5.0×10^{-5}	cm^2sr eV/eV counts/ion
$\Delta E/E$ (FWHM)	1	0.145	eV/eV
$\Delta\alpha$ (FWHM)	1	7.4	deg
$\Delta\beta$ (FWHM)	1	5.1	deg

from all three polar angle detectors are summed together and assigned to the rate scalers on the basis of mass only.

Calibration

Calibration of LOMICS was carried out at Los Alamos National Laboratory using seven ion species at energies between 1 and 30 keV. All three look directions were calibrated by sweeping the sensor through polar and azimuthal angles and varying the ESA plate voltage at each angle. Calibration data for mass peak location (needed by the DPU) were reduced to a set of coefficients (A, B) for the power-law equation

$$T = AE^{-B} \tag{2}$$

Figure 2 shows LOMICS flight data (plotted as E vs T rather than T vs E) together with the fitted calibration data for the lower and upper 10% bounds on the mass peaks.

Although Fig. 2 does not convey the full information of a color spectrogram, one can see that the H^+ peak is shifted slightly toward longer times relative to calibration data, whereas He^+, O^{++}, and O^+ fall within the calibration curves. Mislocation of the H^+ peak can be corrected by uploading a new set of curves that corrects the DPU identification of H^+. Other results of laboratory calibration are summarized in Table 1.

The geometric factor G in Table 1 is defined in the usual way

$$G = A\Omega T\epsilon(\Delta E/E) \quad [cm^2sr] \tag{3}$$

where A is the effective acceptance area (0.29 cm^2), Ω the acceptance solid angle (sr), T the sensor transmission, ϵ the detection efficiency (counts/ion), and $\Delta E/E$ the energy resolution.

Initial On-Orbit Results

LOMICS was switched on at 0830 UT, August 26, 1991 (CRRES orbit 77). Only the first four orbits (77–80) have been examined in any detail. Data in Fig. 3 were taken at nearly the same time as that of Fig. 2, when CRRES was at $L \sim 4.0$ and a local time of 1000. The two curves represent O^+ and H^+ counting rates plotted against time for the energy range 26–32 keV/e. Arrows indicate the (assumed) magnetic field direction, while the peaks in ion fluxes are oriented at 90 deg to this direction. The ions represent a trapped population which is the most common distribution observed by LOMICS in the first four orbits.

Shortly after the first four orbits, LOMICS suffered an intermittent loss of control in the -10.0 kV power supply over a period of approximately six months. Examination of the data shows that loss of the -10.0 kV bias potential was not due to high-voltage break down (which would create detector noise and a number of other symptoms that are not observed) but rather to a variation in the reference voltage to the supply. Fortunately, in June 1991, LOMICS began to operate normally again, possibly because the offending electronic component had been annealed by the accumulated radiation dose. Such recoveries of functionality, while rare, are not unheard of.

Acknowledgments

Design, fabrication, and test of LOMICS has been supported by the Department of Energy. Support for D. Young since 1988 has also been provided by Southwest Research Institute, San Antonio, Texas. This paper is dedicated to Jim Cessna who was responsible for developing the time-of-flight circuitry that forms the electronic heart of LOMICS. We also wish to thank B. Baldonado, W. Feldman, T. Fritz, M. Herrin, J. Longmire, R. Martin, B. Nordholt, N. Olivas, G. Sandoval, and B. Williford of the Los Alamos National Laboratory, Los Alamos, New Mexico, and R. Koga, N. Katz, and S. Imamoto of The Aerospace Corporation, Los Angeles, California, for their contributions to LOMICS design, fabrication, and testing over the past eight years.

References

[1]Cornwall, J. M., "Magnetospheric Ion Acceleration Processes," *Ion Acceleration in the Magnetosphere and Ionosphere,* ed. by T. Chang, American Geophysical Union Monograph Series, American Geophysical Union, Washington, DC, Vol. 38, 1986, pp. 3–16.

[2]Young, D. T., "Experimental Aspects of Ion Acceleration in the Earth's Magnetosphere," *Ion Acceleration in the Magnetosphere and Ionosphere,* ed. by T. Chang, American Geophysical Union Monograph Series, American Geophysical Union, Washington, DC, Vol. 38, 1986, pp. 17-35.

[3]Goldstein, R., and Neugebauer, M. N., "Advanced Techniques for Plasma Composition and Dynamics Measurements," *Advances in Space Research,* Vol. 2, No. 10, 1983, pp. 271–281.

[4]Gloeckler, G., "Ion Composition Measurement Techniques for Space Plasmas," *Review of Scientific Instruments,* Vol. 61, No. 11, 1990, pp. 3613-3620.

[5]Wilken, B., Fritz, T. A., and Studemann, W., "Experimental Techniques for Ion Composition Measurements in Space," *Nuclear Instruments and Methods,* Vol. 196, 1982, pp. 161–167.

[6]Fritz, T. A., Cessna, J. R., and Vigil, R. P., "The CRRES AFGL 701-11B Heavy Ion Telescope Instrument," *Journal of Spacecraft and Rockets,* available from the authors.

[7]Koga, R., Imamoto, S. S., Katz, N., and Pinkerton, S. D., "Data Processing Units for Eight Magnetospheric Particles and Field Sensors," *Journal of Spacecraft and Rockets,* Vol. 29, No. 4, 1992, pp. 574–579.